IOP Publishing Semiconductor Science and Technology
Semicond. Sci. Technol. 31 (2016) 025011 (10pp) doi:10.1088/0268-1242/31/2/025011

A comprehensive study of charge trapping in organic field-effect devices with promising semiconductors and different contact metals by displacement current measurements

Sibani Bisoyi[1,2], Reinhold Rödel[2], Ute Zschieschang[2], Myeong Jin Kang[3], Kazuo Takimiya[4], Hagen Klauk[2] and Shree Prakash Tiwari[1]

[1] Department of Electrical Engineering, Indian Institute of Technology Jodhpur, Rajasthan 342011, India
[2] Max Planck Institute for Solid State Research, Heisenbergstr. 1, D-70569 Stuttgart, Germany
[3] Department of Applied Chemistry, Hiroshima University, Higashi-Hiroshima 739-8527, Japan
[4] RIKEN Centre for Emergent Matter Science (CEMS), Wako, Saitama 351-0198, Japan

E-mail: sptiwari@iitj.ac.in

Received 6 October 2015, revised 24 November 2015
Accepted for publication 25 November 2015
Published 21 December 2015

Abstract

A systematic and comprehensive study on the charge-carrier injection and trapping behavior was performed using displacement current measurements in long-channel capacitors based on four promising small-molecule organic semiconductors (pentacene, DNTT, C_{10}-DNTT and DPh-DNTT). In thin-film transistors, these semiconductors showed charge-carrier mobilities ranging from 1.0 to 7.8 $cm^2\,V^{-1}\,s^{-1}$. The number of charges injected into and extracted from the semiconductor and the density of charges trapped in the device during each measurement were calculated from the displacement current characteristics and it was found that the density of trapped charges is very similar in all devices and of the order 10^{12} cm^{-2}, despite the fact that the four semiconductors show significantly different charge-carrier mobilities. The choice of the contact metal (Au, Ag, Cu, Pd) was also found to have no significant effect on the trapping behavior.

Keywords: thin-film transistors, charge trapping, organic semiconductors, displacement current measurements

(Some figures may appear in colour only in the online journal)

1. Introduction

Organic thin-film transistors (TFTs) are field-effect transistors in which the semiconductor is a thin layer of conjugated organic molecules. The principle of operation is to some extent similar to that of silicon metal-oxide-semiconductor field-effect transistors (MOSFETs): in both devices, the magnitude of the electric current flowing through the semiconductor is controlled by the gate field and can to first order be described by the same formalism [1]. The physical mechanisms, however, are notably different. For example, the charge-carrier channel in a silicon MOSFET is formed by the inversion of the doped semiconductor near the gate-dielectric interface, i.e., the charge carriers forming the channel originate from the semiconductor, and they remain in the semiconductor when the channel is switched off. In contrast, organic semiconductors usually have vanishingly small carrier densities, so the formation of a channel in the semiconductor requires the injection of the necessary charges from the source/drain contacts, and when the channel is removed, the charges are extracted through the contacts. This makes it possible to directly measure the number of charges forming the accumulation channel, the number of charges released during channel annihilation, and (by subtracting one from the other) the number of charges being trapped into localized electronic states. Since charge-carrier trapping during device

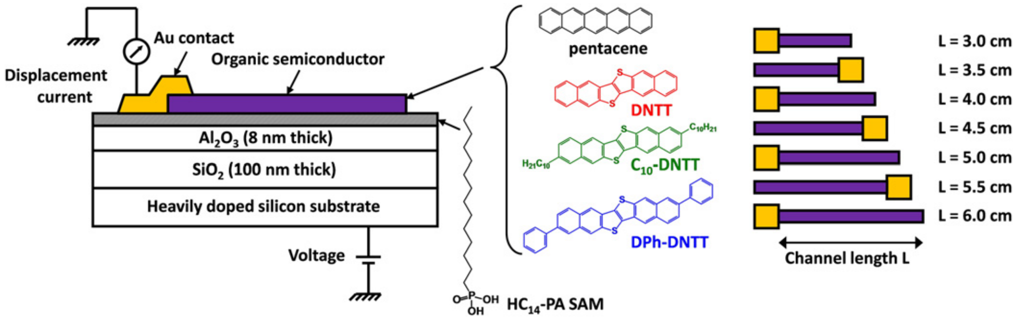

Figure 1. Schematic cross-section and layout of the long-channel capacitors (LCCs). The chemical structures of *n*-tetradecylphosphonic acid (HC_{14}-PA) and of the organic semiconductors pentacene, DNTT, C_{10}-DNTT and DPh-DNTT are also shown.

operation has a significant influence on the device reliability [2, 3], a better quantitative understanding of the trapping dynamics in organic TFTs is of substantial interest.

A particularly useful method for this purpose is the displacement current measurement (DCM), which was first introduced to organic TFTs by Ogawa *et al* [4–8] and later substantially extended by the groups of Ruden and Frisbie [9–13]. In the DCM method, the transistor is biased like a metal–insulator–semiconductor capacitor, i.e., a voltage that slowly changes in magnitude is applied between the gate electrode and a metal contact that is in direct contact with the semiconductor. This time-dependent change of the applied voltage causes a displacement current to flow into (and out of) the semiconductor through the metal contact, and this displacement current is continuously measured at the contact. In principle, a DCM configuration with two metal contacts (source and drain, as in a transistor) is also feasible; in this case, the measurement can be conducted either by shorting the two contacts [4–8] or by applying an additional drain–source voltage and measuring the displacement currents at the source contact and at the drain contact independently and simultaneously, which allows additional insight into the individual potential drops at the various interfaces of the device [14, 15].

In the simplest and perhaps most intuitive DCM configuration, only one metal contact is fabricated and all charges are injected and extracted through this contact [10–13]. In addition, by using devices with very long channels, the displacement currents and transit times can be made sufficiently long to obtain large signal-to-noise ratios during the measurements, and this device configuration is termed long-channel capacitor (LCC) [10].

In most previous reports of DCMs on organic TFTs or LCCs [5, 10–15], the measurements were performed on devices based on the same organic semiconductor (pentacene), making it difficult to draw conclusions regarding the influence of the choice of the semiconductor on the trapping dynamics. In a few cases [4, 6–8], DCM results obtained from pentacene TFTs were compared with results from poly(3-hexylthiophene) (P3HT) [6, 7] or C_{60} TFTs, [4, 8] but the performance of the latter devices was relatively poor; the P3HT TFTs had a very low carrier mobility ($10^{-4}\,cm^2\,V^{-1}\,s^{-1}$), and the response of the C_{60} TFTs was severely degraded by the ambient air. One report showed DCM results obtained from a tetracene single-crystal FET [9], but again, no comparison with other semiconductors was provided. Hence, a systematic study of trapping dynamics for field-effect devices with various new promising semiconductors is required to investigate the trapping behavior.

To investigate how the trapping behavior probed by the DCM method is influenced by the choice of the organic semiconductor, we have fabricated and characterized LCCs based on four different small-molecule semiconductors: pentacene, dinaphtho[2,3-b:2′,3′-f]thieno[3,2-b]thiophene (DNTT [16]), 2,9-didecyl-DNTT (C_{10}-DNTT [17, 18]) and 2,9-diphenyl-DNTT (DPh-DNTT [19]). All of these semiconductors have previously demonstrated great promise for the realization of organic *p*-channel TFTs with excellent static and dynamic performance and stability on flexible plastic substrates [20–27], but they have notably different carrier mobilities, ranging from $1.0\,cm^2\,V^{-1}\,s^{-1}$ (pentacene) to $7.8\,cm^2\,V^{-1}\,s^{-1}$ (DPh-DNTT), as shown in figure 7. One of the questions to be addressed with this experiment is whether these differences in the observed carrier mobilities are reflected in the density of trapped charges that is probed by the DCMs. In addition to using four different semiconductors, we have also employed four different contact metals (Au, Ag, Cu, Pd) in order to investigate whether the choice of the contact metal has an influence on the trapping behavior. In pentacene LCCs, Liang *et al* [12] have previously observed a significantly smaller density of trapped charges when Cu, as opposed to Au, was used as the contact metal.

2. Device fabrication

The schematic cross-section and the layout of the LCCs are shown in figure 1. The LCCs were fabricated on heavily doped silicon substrates, with the substrate also serving as the gate electrode. The gate dielectric is a combination of a 100 nm thick layer of silicon dioxide (grown by dry thermal oxidation), an 8 nm thick layer of aluminum oxide (deposited by atomic layer deposition), and a 1.7 nm thick self-assembled monolayer of *n*-tetradecylphosphonic acid (HC_{14}-PA SAM; obtained by immersing the substrate into a 2-propanol solution of the phosphonic acid). The total thickness of the $SiO_2/Al_2O_3/SAM$ gate dielectric is 110 nm, and it has a capacitance per unit area of $34\,nF\,cm^{-2}$ [18]. Onto this gate dielectric, a 25 nm thick layer of the organic semiconductor was deposited in vacuum through a shadow mask, so that seven LCCs with a channel width of 0.3 cm and with channel lengths ranging from 3 to 6 cm (i.e., with channel areas ranging from 0.9 to 1.8 cm^2) were obtained on each substrate. During the semiconductor depositions, the substrates were held at a temperature of 60 °C–80 °C, depending on the semiconductor. The chemical structures of the four semiconductors, pentacene, DNTT, C_{10}-DNTT and DPh-DNTT, are also shown in figure 1. The LCCs were completed by depositing a 30 nm thick metal contact (Au, Ag, Cu or Pd) near one end of each LCC by thermal evaporation in vacuum through another shadow mask. The metal contacts have an area of 0.5 cm^2 and form a small overlap area with the organic semiconductor layer. The DCMs were performed using an Agilent 4156C Semiconductor Parameter Analyzer, with one source-measure unit (SMU) connected to the gate electrode to apply the voltage and a second SMU connected to the metal contact to measure the displacement current. The same process flow was used to fabricate bottom-gate, top-contact TFTs by depositing the Au source and drain contacts through a shadow mask onto the organic semiconductor layer, defining a channel length of 100 μm and a channel width of 200 μm. All measurements were carried out in ambient air at room temperature and without encapsulation of the devices.

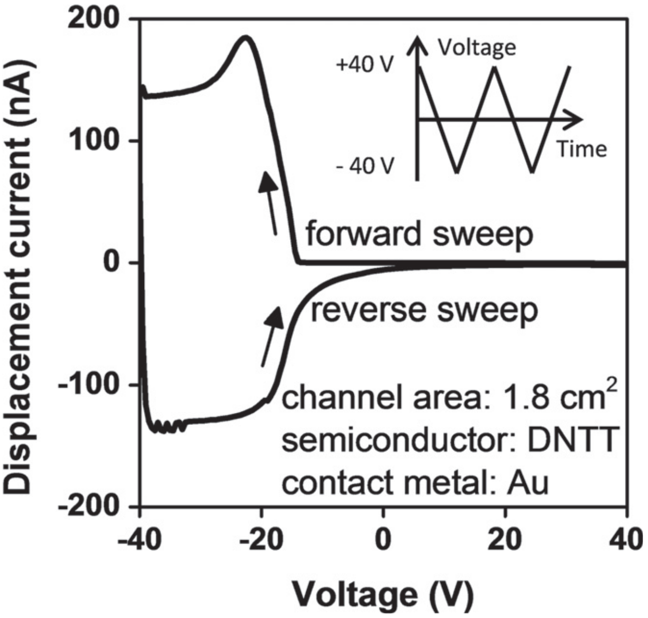

Figure 2. Displacement current measured on an LCC with a channel area of 1.8 cm^2 and with DNTT as the semiconductor and Au as the contact metal. The inset shows the waveform of the voltage applied between the gate electrode and the metal contact of the LCCs during the displacement current measurements, with the metal contact held at ground potential. The voltage is ramped from +40 to −40 V and back from −40 to +40 V with a rate of 1.5 V s^{-1}.

3. Result and discussion

3.1. General considerations

During the DCMs, the metal contact is held at ground potential and the voltage applied between the gate electrode and the metal contact is first ramped from +40 to −40 V and then back from −40 to +40 V, always with a constant rate of 1.5 V s^{-1}. Figure 2 shows the displacement current measured at the metal contact as a function of the applied voltage; this particular measurement was performed on an LCC with a channel area of 1.8 cm^2 (channel length of 6 cm) and with DNTT as the semiconductor and Au as the contact metal. As can be seen, when the applied voltage is ramped from +40 V towards more negative values (forward sweep), the displacement current initially has a small, constant, positive value. In this regime, the semiconductor is devoid of mobile charges (i.e., there is no accumulation channel), so changing the applied voltage affects only the amount of charge on the capacitance formed by the geometric overlap between the metal contact and the gate electrode, and so the displacement current in this regime (below the threshold voltage V_{th}) is determined solely by the capacitance formed between the metal contact and the gate electrode [10]:

$$I_{\mathrm{below}-V_{\mathrm{th}}} = \frac{\partial Q_{\mathrm{contact}}}{\partial t} = -C_{\mathrm{contact}}\frac{\partial V}{\partial t} = -A_{\mathrm{contact}}\, C''_{\mathrm{diel}}\frac{\partial V}{\partial t}, \qquad (1)$$

where Q_{contact} is the charge flowing into or out of the region underneath the metal contact, t is the time, C_{contact} is the capacitance formed between the metal contact and the gate electrode, $\partial V/\partial t$ is the voltage sweep rate (1.5 V s^{-1}), A_{contact} is the area of the metal contact (0.5 cm^2), and C''_{diel} is the gate-dielectric capacitance per unit area (34 nF cm^{-2}). Note that changing the applied voltage towards more negative (positive) values produces a positive (negative) displacement current, due to the fact that the potential change acts on the gate electrode, while the displacement current is measured at the metal contact. According to equation (1), the displacement current in the regime in which the semiconductor is devoid of mobile charges should be about 25 nA. According to figure 2, the displacement current actually measured in this regime is about 1 nA. The reason for the discrepancy between the calculated and measured values is not known.

When the applied voltage reaches the threshold voltage (−14 V), a sharp increase in the measured displacement current indicates the sudden injection of a large number of positive charges from the metal contact into the semiconductor. These charges spread across the entire semiconductor area and form an accumulation channel near the semiconductor/dielectric interface that balances the negative charge on the gate electrode (more precisely, the portion of the gate charge that is not already balanced by fixed or trapped charges in the gate dielectric or at the interface). The formation of this accumulation channel requires that the injected charges are transported from the metal contact in a lateral direction parallel to the dielectric interface towards the end of the semiconductor region, so the time required to complete the formation of the channel (and hence the slope of the increase of the measured displacement-current upon sweeping the gate potential towards more negative values) depends on the charge-carrier mobility and on the channel length ($L = 6\,\text{cm}$ in this particular device) [10].

Once the formation of the accumulation channel is completed, the displacement current decreases to a constant, positive value that is determined by the total capacitance formed by combination of the metal contact and the accumulation channel on one side and the gate electrode on the other side [10]:

$$I_{\text{above}-V_{\text{th}}} = \frac{\partial\left(Q_{\text{contact}} + Q_{\text{channel}}\right)}{\partial t} = -\left(A_{\text{contact}} + A_{\text{channel}}\right) C''_{\text{diel}} \frac{\partial V}{\partial t}, \qquad (2)$$

where Q_{channel} is the charge flowing into or out of the channel to balance the voltage-dependent gate charge and A_{channel} is the area of the semiconductor channel ($1.8\,\text{cm}^2$ in this particular device). In this regime, any change of the applied voltage will change the amount of charge in the accumulation channel, and since the area of the channel is much larger than the area of the metal contact ($A_{\text{channel}} > A_{\text{contact}}$), the displacement current in this regime will be much larger than the displacement current measured below the threshold voltage. According to equation (2), the displacement current in the above-threshold regime should be about 120 nA, and according to figure 2, the displacement current actually measured in this regime is about 140 nA, in reasonable agreement with the calculated value.

When the applied voltage is ramped back from $-40\,\text{V}$ towards more positive values (reverse sweep), the amount of negative gate charge is monotonically decreased and thus the number of positive charges in the channel also decreases monotonically, which means that excess positive charges are extracted from the semiconductor through the metal contact. Thus, the displacement current in this regime is negative, but provided the voltage ramp rate has the same magnitude as during the forward sweep (which is the case here), the magnitude of the displacement current is also the same as during the forward sweep, as given by equation (2). Once the voltage applied during the reverse sweep reaches the threshold voltage ($-14\,\text{V}$), the accumulation channel disappears, the device capacitance is reduced to the capacitance of the metal contact, and thus the magnitude of the displacement current decreases and eventually reaches a small, constant, negative value, given by equation (1). There are two aspects in which the shape of the displacement–current versus gate–voltage curve measured during the reverse sweep differs from that measured during the forward sweep: one is that the annihilation of the accumulation channel does not produce a sharp peak in the displacement current, as was the case during the formation of the accumulation channel during the forward sweep. The other is that the drop in the displacement current upon annihilation of the accumulation channel during the reverse sweep is less abrupt and more gradual than the increase in the displacement current upon formation of the accumulation channel during the forward sweep. This gradual decrease of the displacement current in the reverse sweep is due to the delayed emission of trapped charges during or following the annihilation of the channel [10, 11].

By integrating the measured displacement current over the applied voltage and multiplying with the inverse of the voltage sweep rate, the number of charges injected into the semiconductor during the forward sweep (N_{injected}) and the number of charges extracted from the semiconductor during the reverse sweep ($N_{\text{extracted}}$) can be calculated [10]:

$$N_{\text{injected}} = \left| \frac{1}{q} \left(\frac{\partial V}{\partial t}\right)^{-1} \int_{V_{\text{start}}}^{V_{\text{end}}} \left(I_{\text{forward}} - I_{\text{below}-V_{\text{th}}}\right) \mathrm{d}V \right|, \qquad (3)$$

$$N_{\text{extracted}} = \left| \frac{1}{q} \left(\frac{\partial V}{\partial t}\right)^{-1} \int_{V_{\text{end}}}^{V_{\text{start}}} \left(I_{\text{reverse}} - I_{\text{below}-V_{\text{th}}}\right) \mathrm{d}V \right|, \qquad (4)$$

where q is the electronic charge, $\partial V/\partial t$ is the voltage sweep rate, V_{start} and V_{end} are the voltages at the beginning and the end of the forward and reverse sweeps ($V_{\text{start}} = +40\,\text{V}$; $V_{\text{end}} = -40\,\text{V}$), I_{forward} and I_{reverse} are the displacement currents measured during the forward and reverse sweep, and $I_{\text{below-}V\text{th}}$ is the displacement current measured below the threshold voltage in the absence of an accumulation channel. By subtracting the number of charges extracted from the semiconductor during the reverse sweep ($N_{\text{extracted}}$) from the number of charges injected into the semiconductor during the forward sweep (N_{injected}), the number of charges being trapped in the device during the forward and reverse sweep (N_{trapped}) can be calculated [10]:

$$N_{\text{trapped}} = N_{\text{injected}} - N_{\text{extracted}}. \qquad (5)$$

Since the number of charges being trapped during the measurement is expected to depend not only on the materials properties, but also on the device geometry, it is useful to normalize N_{trapped} with respect to the device geometry. Figure 3 summarizes the results of DCMs performed on LCCs in which the channel length was varied from 3 to 6 cm, which means that the area of the organic semiconductor varied from 0.9 to $1.8\,\text{cm}^2$. In figure 3(a) it can be seen that the magnitude of the displacement current measured below the threshold voltage is independent of the semiconductor area, which is in agreement with the fact that the displacement current in this regime is determined only by the overlap area between the metal contact and the gate electrode, not by the area of the semiconductor; see equation (1). In contrast, the magnitude of the displacement current measured above the threshold voltage shows a monotonic dependence on the semiconductor area, which is in agreement with equation (2). In figure 3(b), the numbers of injected, extracted and trapped charges calculated using equations (3)–(5) are plotted as a function of the semiconductor area. As can be seen, all three parameters increase approximately linearly with the semiconductor area, indicating that the charge distribution across the semiconductor area is approximately homogeneous. It is therefore reasonable to normalize the number of trapped charges (N_{trapped}) with respect to the area of the organic semiconductor ($A_{\text{semiconductor}}$) and define an effective density of

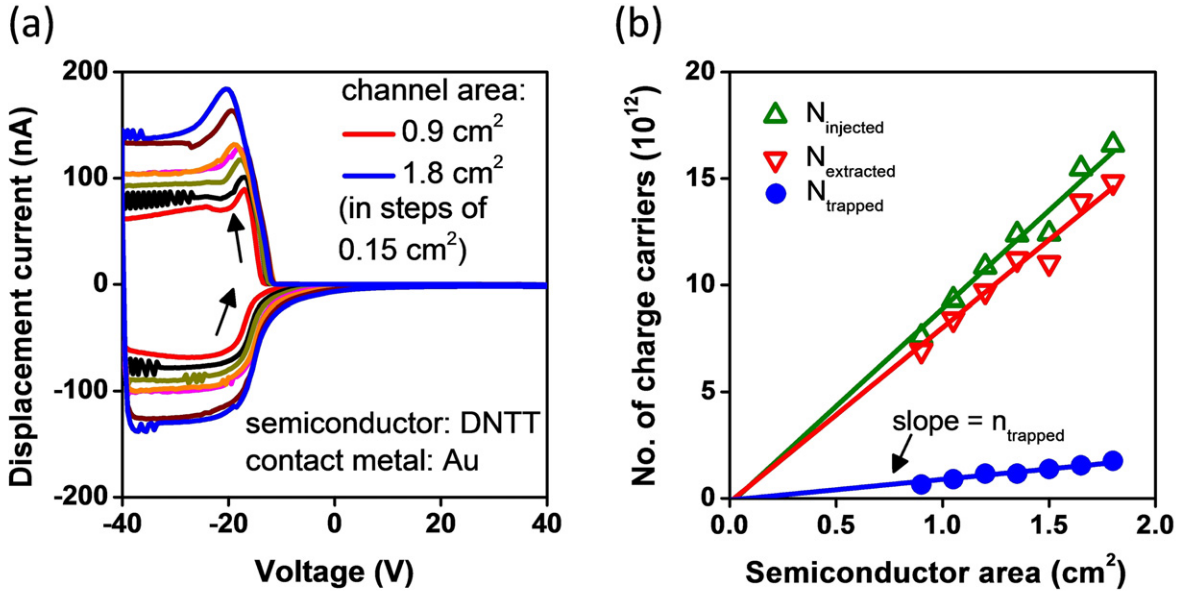

Figure 3. (a) Displacement currents measured on LCCs with semiconductor areas ranging from 0.9 to 1.8 cm^2. All curves from the first sweep. (b) Number of charges injected during the forward sweep (N_{injected}), extracted during the reverse sweep ($N_{\text{extracted}}$) and trapped during forward and reverse sweep ($N_{\text{trapped}} = N_{\text{injected}} - N_{\text{extracted}}$) as a function of the semiconductor area. All three parameters increase approximately linearly with the semiconductor area.

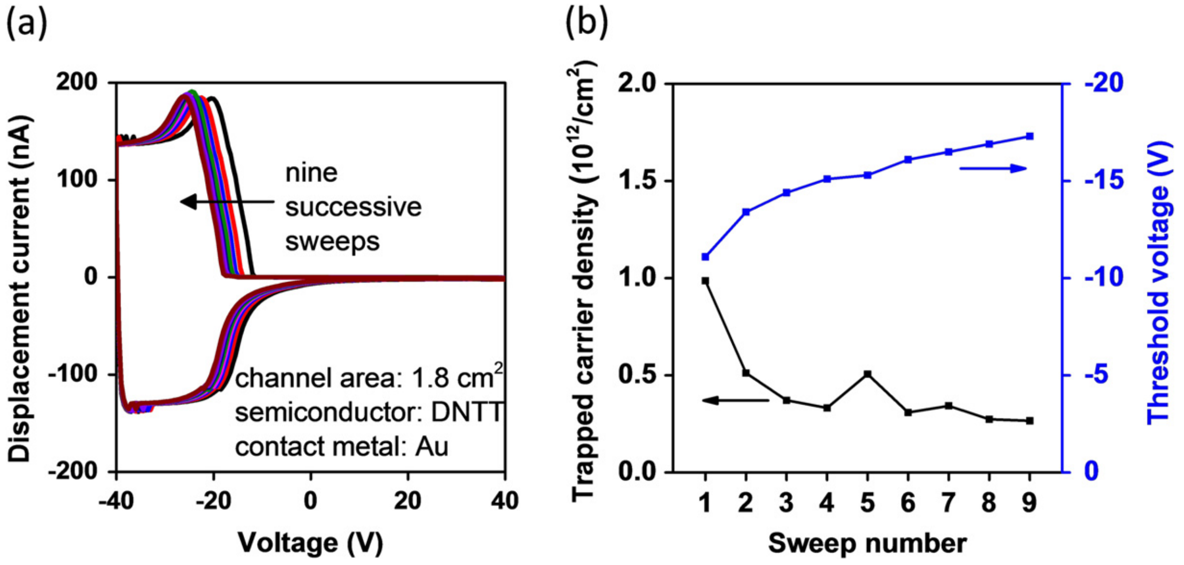

Figure 4. (a) Displacement current measured during nine successive forward and reverse sweeps. (b) Threshold voltage estimated from the onset of the peak in the displacement current measured during the forward sweep of nine successive measurements, and density of trapped charges during each of nine successive measurements. With each successive measurement, the threshold voltage shifts towards more negative values, until it saturates.

trapped charges (n_{trapped}):

$$n_{\text{trapped}} = \frac{N_{\text{trapped}}}{A_{\text{semiconductor}}}. \tag{6}$$

3.2. Threshold-voltage shift during repeated measurements

Figure 4(a) shows that when the DCM is repeated several times, the threshold voltage shifts by a few volts towards more negative values (see also figure 4(b)). This shift of the threshold voltage during repeated measurements was also observed by Liang *et al* [10, 12] and was ascribed to the filling of more and more deep trap states during each measurement. Charges trapped in deep states remain inside the device after the completion of the measurement and affect the threshold voltage observed during the following measurement. As more and more deep states are filled, the density of deep states available in the device is expected to decrease with each measurement. Indeed, using equations (3)–(6) we find that the density of charges trapped during each measurement decreases from $10^{12}\,\mathrm{cm}^{-2}$ during the first measurement to $3 \times 10^{11}\,\mathrm{cm}^{-2}$ during the ninth measurement (see figure 4(b)). These values are larger by an order of magnitude than those reported by Liang *et al* [10]. However, it should be noted that a different gate dielectric and different organic semiconductors were used in these two studies, which will result in different trapping densities. Also, in our measurements the gate-induced charge density is about two times larger and the duration of each measurement is about four times longer than in the measurements reported by Liang *et al* and both of these parameters are likely to affect the trapping probability.

Assuming that all charges trapped during a particular measurement are still in deep states at the beginning of the following measurement, the threshold-voltage shift expected to be induced by these trapped charges can be calculated as follows:

$$\Delta V_{\mathrm{th}} = \frac{q\, n_{\mathrm{trapped}}}{C''_{\mathrm{diel}}}. \tag{7}$$

However, the measured threshold-voltage shifts are on average a factor of two to three smaller than the threshold-voltage shifts calculated using equation (7). For example, the density of charges trapped during the first measurement is $1 \times 10^{12}\,\mathrm{cm}^{-2}$, which, according to equation (7), would be expected to induce a threshold-voltage shift of 4.6 V, but the measured shift from the first to the second measurement is only 2.3 V. This indicates that approximately one half to two thirds of the charges trapped during each measurement are released before the beginning of the following measurement, which suggests that some of the traps have characteristic lifetimes that are shorter than the duration of a single measurement.

3.3. Choice of the semiconductor

To see how the density of trapped charges probed by the DCMs is influenced by the choice of the organic semiconductor, we have fabricated LCCs based on four different small-molecule semiconductors: pentacene, DNTT, C_{10}-DNTT and DPh-DNTT. All of these semiconductors have previously demonstrated great promise for the realization of organic *p*-channel TFTs with good static and dynamic performance and stability on flexible plastic substrates [20–27], but they have notably different carrier mobilities, ranging from $1.0\,\mathrm{cm}^2\,\mathrm{V}^{-1}\,\mathrm{s}^{-1}$ (pentacene) to $7.8\,\mathrm{cm}^2\,\mathrm{V}^{-1}\,\mathrm{s}^{-1}$ (DPh-DNTT) as obtained from our TFTs (see figure 7). One of the questions to be addressed with this experiment is whether these differences in the observed carrier mobilities are reflected in the density of trapped charges that is probed by the DCMs.

Figure 5(a) shows the displacement–current versus gate–voltage curves measured on LCCs based on all four semiconductors, all with a channel area of $1.5\,\mathrm{cm}^2$ and with Au as the contact metal. According to equations (1) and (2), the displacement currents measured well below and well above the threshold voltage are expected to be independent of the choice of the semiconductor, and indeed they are very similar in all four curves. In contrast, the displacement current measured in the transition regions near the threshold voltage, both in the forward and in the reverse sweep, is expected to be greatly affected by the carrier mobility and by the trapping dynamics [10]. Indeed, in the transition regions small differences between the four curves can be discerned.

Using equations (3)–(6), we have calculated the number of charges injected and extracted during the forward and reverse sweeps (N_{injected}, $N_{\mathrm{extracted}}$) and the number and the density of charges trapped during the DCMs (N_{trapped}, n_{trapped}). The results for all four semiconductors are summarized in table 1. Also included in table 1 are the threshold voltage V_{th} (estimated from the onset of the peak associated with the formation of the accumulation channel during the forward sweep), the carrier mobility estimated from the slope of that peak (μ_{DCM}) [10], and the carrier mobility calculated from current–voltage measurements performed on TFTs (μ_{TFT}) based on the same semiconductors and fabricated on the same type of substrate ($\mathrm{Si/SiO_2/Al_2O_3/SAM}$) with the same film thicknesses and also using a top-contact device structure [18]. Transfer characteristics, output characteristics and differential charge-carrier mobility as a function of gate-source voltage of these TFTs are shown in figure 7.

In figures 5(b) and (c), the values calculated for N_{injected}, $N_{\mathrm{extracted}}$ and n_{trapped} are plotted versus the carrier mobility estimated from the DCMs. As can be seen, N_{injected}, $N_{\mathrm{extracted}}$ and n_{trapped} are all very similar for the four semiconductors, despite the significant differences in carrier mobility. In particular, no systematic trend between the density of trapped charges and the carrier mobility can be discerned. This is somewhat surprising, considering that it is commonly believed that the charge-carrier mobility in organic semiconductors is at least to some extent limited by charge-carrier trapping.

A possible explanation is that the differences between the charge-carrier mobilities in the four semiconductors are caused by trapping events that have characteristic lifetimes which are shorter than the duration of our DCMs, so that these trapping events remain undetected by our measurements (in other words, the carriers are released from the traps before the end of the measurement). This explanation is in line with the observation that the charge-carrier mobility in organic semiconductors is limited mainly by shallow traps [28], i.e., by traps that have small activation energies (approximately 0.1–0.2 eV for the semiconductors investigated in [28]) and hence short characteristic lifetimes (as opposed to bias-stress-induced threshold-voltage shifts, which are more likely caused by trapping in deep states with long characteristic lifetimes [2, 3]). An alternative explanation is that the differences in carrier mobility are not primarily due to differences in the density of charges being trapped, but due to secondary effects resulting from the trapping events (e.g., differences in the scattering cross-sections of the filled trap states depending on the trap energy), or due to effects that are not at all related to charge-carrier trapping, but perhaps to differences in the transfer integrals or reorganization energies of the molecules [29–32] or to charge-carrier scattering induced by structural or energetic disorder.

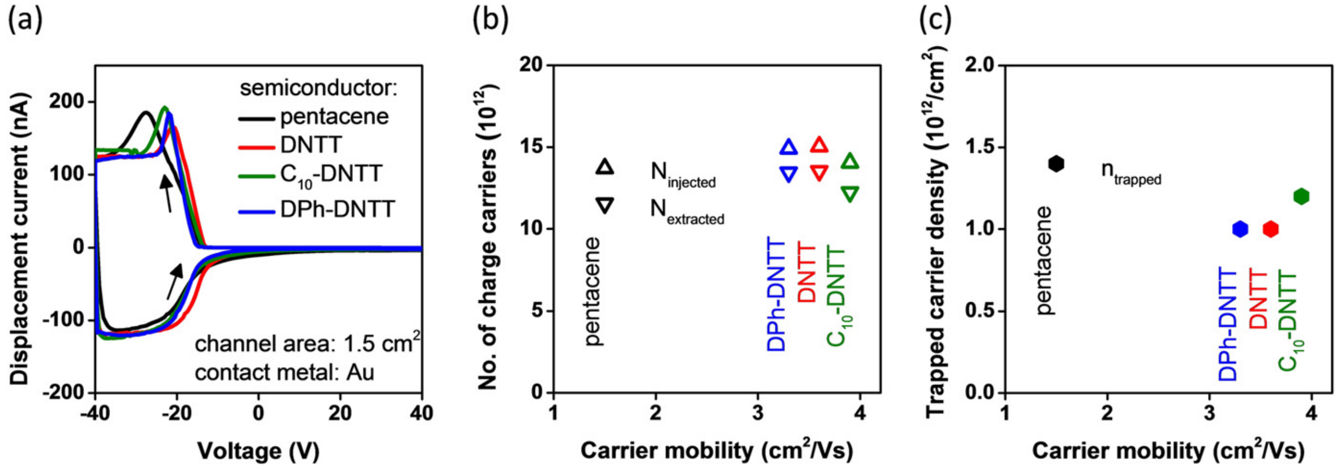

Figure 5. (a) Displacement current measured on LCCs based on all four semiconductors, all with a channel area of 1.5 cm^2 and with Au as the contact metal. All curves from the first sweep. (b) Number of charges injected during the forward sweep (N_{injected}) and extracted during the reverse sweep ($N_{\text{extracted}}$) plotted versus the charge-carrier mobility estimated from the displacement current measurements [10]. The numbers are similar for all semiconductors. (c) Density of charges trapped during the displacement current measurement (n_{trapped}) plotted versus the charge-carrier mobility estimated from the displacement current measurements. No systematic trend between the density of trapped charges and the charge-carrier mobility can be discerned.

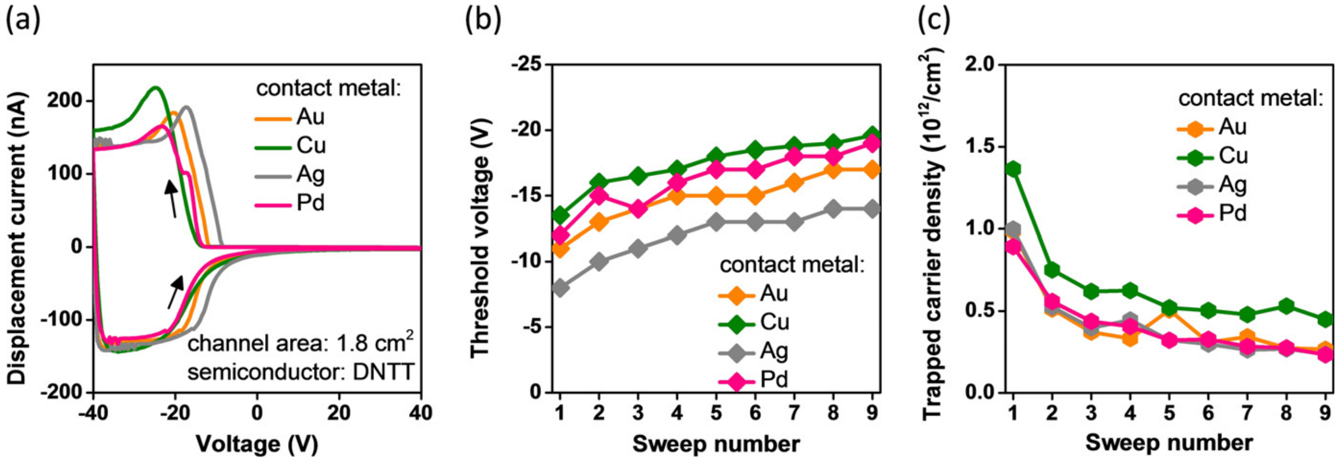

Figure 6. (a) Displacement current measured on LCCs based on Au, Cu, Ag and Pd as the contact metal, all with DNTT as the semiconductor and all with a channel area of 1.8 cm^2. All curves from the first sweep. (b) Threshold voltage estimated from the onset of the peak in the displacement current measured during the forward sweep of nine successive measurements performed on DNTT-based LCCs with either Au, Cu, Ag or Pd as the contact metal. (c) Density of trapped charges during nine successive measurements performed on DNTT-based LCCs with either Au, Cu, Ag or Pd as the contact metal.

Table 1. Numbers of injected, extracted and trapped charges, density of trapped charges, threshold voltage (V_{th}) and charge-carrier mobility (μ_{DCM}) estimated from the displacement current measurements, as well as charge-carrier mobility calculated from TFT measurements (μ_{TFT}).

Semiconductor	N_{injected} (10^{12})	$N_{\text{extracted}}$ (10^{12})	N_{trapped} (10^{12})	n_{trapped} (10^{12} cm^{-2})	$V_{\text{th, DCM}}$ (V)	μ_{DCM} (cm^2 V^{-1} s^{-1})	μ_{TFT} (cm^2 V^{-1} s^{-1})
Pentacene	13.7	11.6	2.1	1.4	−13	1.5	1.0
DNTT	15.0	13.5	1.5	1.0	−10	3.6	4.4
C_{10}-DNTT	14.1	12.2	1.9	1.2	−13	3.9	6.5
DPh-DNTT	15.0	13.4	1.6	1.0	−10	3.3	7.8

3.4. Choice of the contact metal

Finally, we have also evaluated the influence of the choice of the contact metal on the displacement current characteristics. For this experiment, we fabricated and characterized LCCs using DNTT as the semiconductor and gold, copper, silver or palladium as the contact metal. In a similar experiment (using pentacene as the semiconductor), Liang *et al* [12] had previously found that the density of trapped charges is

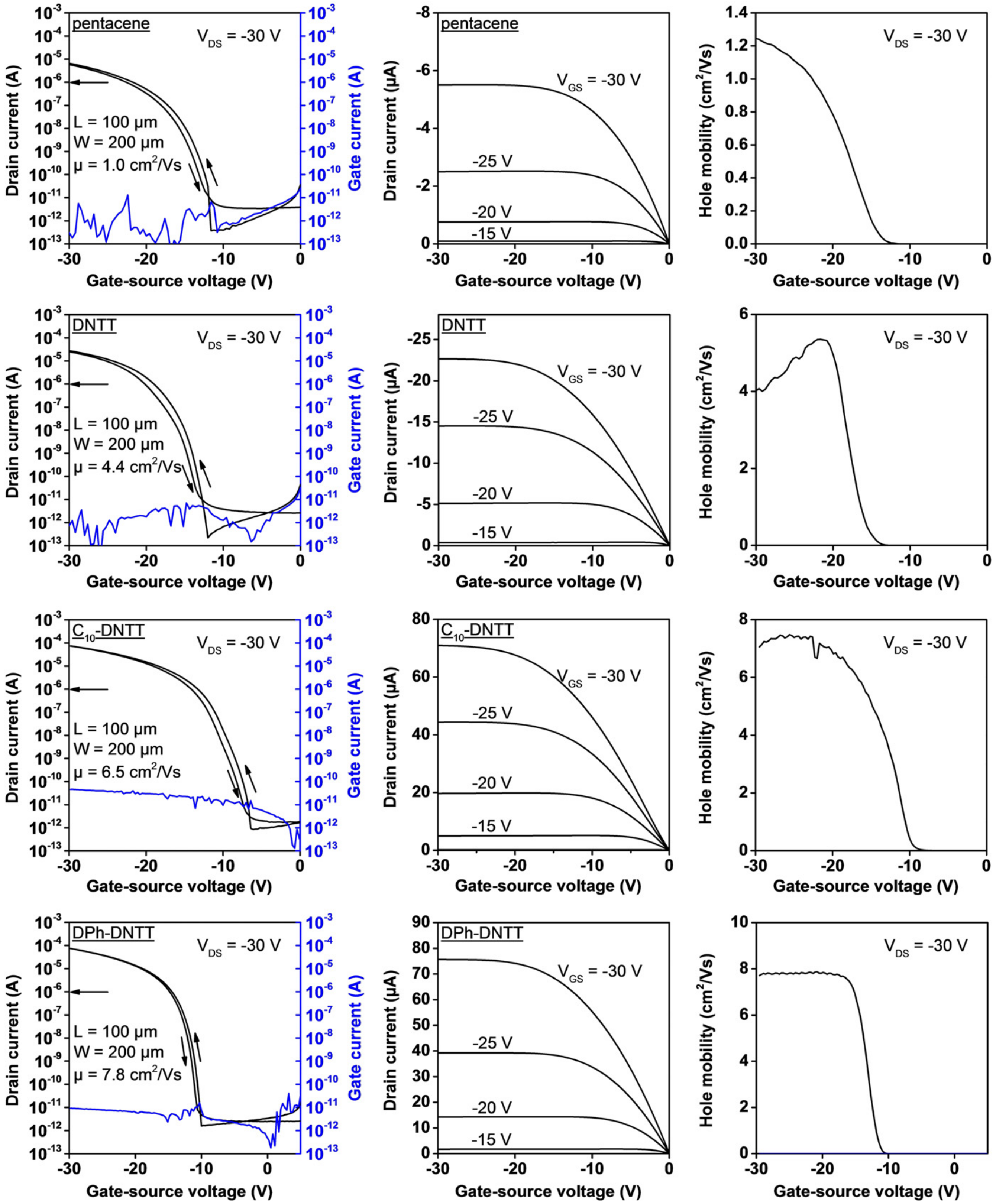

Figure 7. Transfer characteristics, output characteristics and differential charge-carrier mobility as a function of gate-source voltage of pentacene, DNTT, C_{10}-DNTT and DPh-DNTT TFTs.

significantly smaller in LCCs with Cu, as opposed to Au, as the contact metal, which indicates that the choice of the contact metal can have an influence on the density of trapped charges probed by DCMs. Also, several authors, including Wang *et al* [33], have reported that the contact resistance of pentacene TFTs is smaller when Cu, rather than Au, is employed as the contact metal, while Necliudov *et al* [34] reported slightly smaller contact resistances for pentacene TFTs with Au, rather than Pd, as the contact metal. The reason we have chosen DNTT, rather than pentacene, as the semiconductor for our experiment is that DNTT TFTs have been shown to provide larger field-effect mobility and better air stability compared with pentacene TFTs [21]. DNTT TFTs are usually fabricated using Au as the contact metal, although Ag (deposited by inkjet-printing [35], screen-printing [36] or vacuum deposition [37]) has also been successfully employed. Cu and Pd have to our knowledge not been previously employed as the contact metal for DNTT devices.

Figure 6(a) shows the displacement–current versus gate–voltage curves measured on DNTT-based LCCs with a channel area of 1.8 cm^2 and with either Au, Cu, Ag or Pd as the contact metal. The main difference between the curves is the threshold voltage, which varies from -8 V for Ag to -11 V for Au, -12 V for Pd and -13 V for Cu (see also figure 6(b)). The density of charges trapped during each of nine successive DCMs performed on LCCs based on all four contact metals is summarized in figure 6(c). It appears that the choice of the contact metal has only a small influence on the density of trapped charges probed by the DCMs; if anything, the density of trapped charges appears to be slightly larger for Cu than for Au, which is in contrast to the trend reported by Liang *et al* [12], although it should be pointed out again that Liang *et al* employed pentacene, rather than DNTT, as the semiconductor.

4. Conclusions

We have systematically performed DCMs on LCCs based on four promising small-molecule organic semiconductors (pentacene, DNTT, C_{10}-DNTT and DPh-DNTT), all of which show charge-carrier mobilities greater than 1 $cm^2 V^{-1} s^{-1}$. We have found that the density of trapped charges is very similar in all devices, despite the significant differences between the charge-carrier mobilities in the four semiconductors. A possible explanation for the lack of a systematic trend between the charge-carrier mobility and the density of trapped charges in our measurements is that the mobilities are limited by trapping events that remain undetected by the DCMs, perhaps due to significant differences in the trap energies, for example, the mobility is limited by shallow traps, whereas the DCMs detect only trapping in deeper states. An alternative explanation is that the differences in carrier mobility are due to effects other than charge-carrier trapping, such as differences in the scattering cross-sections of the filled trap states depending on the trap energy. It was also found that the choice of the contact metal (Au, Ag, Cu, Pd) does not have any significant effect on the trapping behavior either, which is somewhat less surprising.

Acknowledgments

This work was partially funded by the German Ministry of Education and Research (BMBF) under Grant 1612000463 (KoSiF). S Bisoyi would like to thank Klaus von Klitzing for providing the opportunity to work at the Max Planck Institute for Solid State Research.

References

[1] Marinov O, Deen M J, Zschieschang U and Klauk H 2009 *IEEE Trans. Electron Devices* **56** 2952
[2] Sirringhaus H 2009 *Adv. Mater.* **21** 3859
[3] Bobbert P A, Sharma A, Mathijssen S G J, Kemerink M and de Leeuw D M 2012 *Adv. Mater.* **24** 1146
[4] Ogawa S, Kimura Y, Ishii H and Niwano M 2003 *Japan. J. Appl. Phys.* **42** L1275
[5] Ogawa S, Naijo T, Kimura Y, Ishii H and Niwano M 2005 *Appl. Phys. Lett.* **86** 252104
[6] Ogawa S, Naijo T, Kimura Y, Ishii H and Niwano M 2005 *Synth. Met.* **153** 253
[7] Ogawa S, Naijo T, Kimura Y, Ishii H and Niwano M 2006 *Japan. J. Appl. Phys.* **45** 530
[8] Ogawa S, Kimura Y, Niwano M and Ishii H 2007 *Appl. Phys. Lett.* **90** 033504
[9] Xia Y, Kalihari V, Frisbie C D, Oh N K and Rogers J A 2007 *Appl. Phys. Lett.* **90** 162106
[10] Liang Y, Frisbie C D, Chang H-C and Ruden P P 2009 *J. Appl. Phys.* **105** 024514
[11] Chang H-C, Ruden P P, Liang Y and Frisbie C D 2010 *J. Appl. Phys.* **107** 104502
[12] Liang Y, Chang H C, Ruden P P and Frisbie C D 2011 *J. Appl. Phys.* **110** 064514
[13] Chang H C, Ruden P P, Liang Y and Frisbie C D 2011 *Appl. Phys. Lett.* **99** 073306
[14] Majima Y, Kawakami D, Suzuki S and Yasutake Y 2007 *Japan. J. Appl. Phys.* **46** 39
[15] Suzuki S, Yasutake Y and Majima Y 2008 *Japan. J. Appl. Phys.* **47** 3167
[16] Yamamoto T and Takimiya K 2007 *J. Am. Chem. Soc.* **129** 2224
[17] Kang M J, Doi I, Mori H, Miyazaki E, Takimiya K, Ikeda M and Kuwabara H 2011 *Adv. Mater.* **23** 1222
[18] Hofmockel R *et al* 2013 *Org. Electron.* **14** 3213
[19] Niimi K, Kang M J, Miyazaki E, Osaka I and Takimiya K 2011 *Org. Lett.* **13** 3430
[20] Myny K, Beenhakkers M J, van Aerle N A J M, Gelinck G H, Genoe J, Dehaene W and Heremans P 2011 *IEEE J. Solid-State Circuits* **46** 1223
[21] Zschieschang U *et al* 2011 *Org. Electron.* **12** 1370
[22] Zschieschang U, Kang M J, Takimiya K, Sekitani T, Someya T, Canzler T W, Werner A, B-Nimoth J and Klauk H 2012 *J. Mater. Chem.* **22** 4273
[23] Zschieschang U *et al* 2013 *Org. Electron.* **14** 1516
[24] Yokota T, Kuribara K, Tokuhara T, Zschieschang U, Klauk H, Takimiya K, Sadamitsu Y, Hamada M, Sekitani T and Someya T 2013 *Adv. Mater.* **25** 3639
[25] Glowacki E D *et al* 2013 *Adv. Mater.* **25** 1563
[26] Bisoyi S, Zschieschang U, Kang M J, Takimiya K, Klauk H and Tiwari S P 2014 *Org. Electron.* **15** 3173

[27] Zaki T, Rödel R, Letzkus F, Richter H, Zschieschang U, Klauk H and Burghartz J N 2013 *IEEE Electron Device Lett.* **34** 520

[28] Li C, Duan L, Li H and Li Y Q 2014 *J. Phys. Chem.* C **118** 10651

[29] Cornil J, Calbert J P and Bredas J L 2001 *J. Am. Chem. Soc.* **123** 1250

[30] Troisi A and Orlandi G 2005 *J. Phys. Chem.* B **109** 1849

[31] Coropceanu V, Sanchez-Carrera R S, Paramonov P, Day G M and Bredas J L 2009 *J. Phys. Chem.* C **113** 4679

[32] Sanchez-Carrera R S, Atahan S, Schrier J and Aspuru-Guzik A 2010 *J. Phys. Chem.* C **114** 2334

[33] Wang S D, Minari T, Miyadera T, Tsukagoshi K and Aoyagi Y 2007 *Appl. Phys. Lett.* **91** 203508

[34] Necliudov P V, Shur M S, Gundlach D J and Jackson T N 2003 *Solid-State Electron.* **47** 259

[35] Yokota T *et al* 2011 *MRS Commun.* **1** 3

[36] Peng B and Chan P K L 2014 *Org. Electron.* **15** 203

[37] Ren X and Chan P K L 2014 *Appl. Phys. Lett.* **104** 113302